Crystalline Lamellae and Surface Morphology of Biodegradable Polyhydroxyalkanoate Thin Films: Thermal Behavior and Comparison between Poly(3-hydroxybutyrate-*co*-3-hydroxyhexanoate) and Poly(3-hydroxybutyrate)

Katsuhito Mori,[†] Shota Mukoyama,[†] Ying Zhang,[†] Harumi Sato,[‡] Yukihiro Ozaki,[‡] Hikaru Terauchi,[†] Isao Noda,[§] and Isao Takahashi*,[†]

Department of Physics, Faculty of Science and Technology, Kwansei Gakuin University, Sanda, Hyogo 6691337, Japan; Department of Chemistry, Faculty of Science and Technology, Kwansei Gakuin University, Sanda, Hyogo 6691337, Japan; and The Procter & Gamble Company, 8611 Beckett Road, West Chester, Ohio 45069

Received September 16, 2007; Revised Manuscript Received January 3, 2008

ABSTRACT: We investigate surface morphology and crystalline structure of biodegradable polymers poly(3-hydroxybutyrate) (PHB) and its random copolymer poly(3-hydroxybutyrate-*co*-3-hydroxyhexanoate) (P(HB-*co*-HHx), HHx = 12 mol %) using surface-sensitive techniques. Surface region typically to a depth of about 10 nm of polymer films which have thickness ranging from 20 to 120 nm is observed by grazing incidence X-ray diffraction (GIXD), X-ray reflectivity (XR), and atomic force microscopy (AFM). Both PHB and P(HB-*co*-HHx) show that crystallographic *b*-axis of crystallites in the surface region is aligned in the direction normal to the surface. It indicates that intermolecular interaction along *a*-axis is still dominant in the surface region, which would also determine the fastest growth direction of crystalline lamellae. A lattice relaxation peculiar to P(HB-*co*-HHx) surfaces is recognized in the *b*-axis length. As temperature is raised, crystalline lamellae characterized by densely packed molecular chains appear, implying a thermally activated transformation from metastable lamellae to stable ones. The metastable lamellae in which molecular chains fold loosely are mainly observed throughout rapid cooling, although the loosely and densely packed lamellae equally form in slow cooling. Furthermore, continuous lamellae melting at the surface is observed, all of which suggest an additional process for forming the metastable long-range order in the surface region. Crystallinity at polymer surface would also be responsible for the difference in surface morphology between PHB and P(HB-*co*-HHx) revealed by XR and AFM.

Introduction

Poly(hydroxyalkanoate)s (PHAs) including poly(3-hydroxybutyrate) (PHB) homopolymer and related copolymers are biologically produced, semicrystalline biodegradable polymers which have attracted considerable attention as potential substitutes for petrochemical plastics.[1−5] PHB crystals (a = 0.576 nm, b = 1.32 nm, and c (fiber axis) = 0.596 nm, space group $P2_12_12_1$) are typically distributed as lamellar crystallites in an amorphous matrix.[6,7] Melt temperature (ca.172 °C), which happens to be close to thermal decomposition temperature (ca. 200 °C), and a relatively high degree of crystallinity (it sometimes exceeds 50%) are major obstacles to its practical applications. Poly(3-hydroxybutyrate-*co*-3-hydroxyhexanoate) (P(HB-*co*-HHx)) is a random copolymer comprised of 3-hydroxybutyrate and a minor amount of 3-hydroxyhexanoate units with side groups substituted with a longer propyl chain.[8−10] Melt temperature and crystallinity are substantially reduced by this substitution, and flexibility is significantly improved compared with that of PHB homopolymer. Furthermore, P(HB-*co*-HHx) exhibits some other attractive properties, e.g., anaerobic and aerobic biodegradability, hot alkaline digestibility, hydrolytic stability, good odor and oxygen barrier capability, and excellent surface properties for printing.[11]

In previous studies, structure and thermal behavior of PHB and P(HB-*co*-HHx) crystals in bulk samples were investigated by a combination of wide-angle X-ray diffraction (WAXD) and Fourier transform infrared (FT-IR) spectroscopy.[12−15] Temperature dependence of diffracted X-ray patterns and IR spectra indicated that there is a unique inter- and intramolecular interaction along crystallographic *a*-axis direction, which can be referred to as a weak hydrogen bonding of C−H···O═C type. The presence of such molecular interaction in bulk polymers can, to a certain extent, explain the difference in melting behaviors between PHB and P(HB-*co*-HHx).

An intensive X-ray diffraction and AFM study on crystalline structure and surface morphology of PHB homopolymer thin films at room temperature was recently reported, in which thickness of PHB films ranged from tens of nanometers to micrometers.[16] Nevertheless, little has been known about the molecular structure of lamellae in surface region and surface morphology near the melting point of P(HB-*co*-HHx) as well as those of the homopolymer. Research on the surface structure and morphology of polymeric compounds close to their melting point would certainly be crucial to understand the nature of melting of crystalline lamella, crystallization, and transformation to the glassy state. For non-polymeric substances, the onset of melting is believed to occur at the surface where a quasi-liquid layer is formed at a temperature substantially below the bulk melting point.[17] As for the crystallization in non-polymeric glassy substances, it often occurs from the surface region where a higher molecular mobility peculiar to the surface can promote the crystal growth.[18] Information on surface melting and crystallization in polymers would also be important for practical applications, since physical properties of films, coating, and

* Corresponding author. E-mail: suikyo@kwansei.ac.jp.
† Department of Physics, Kwansei Gakuin University.
‡ Department of Chemistry, Kwansei Gakuin University.
§ The Procter & Gamble Company.

10.1021/ma7020858 CCC: $40.75
Published on Web 02/16/2008

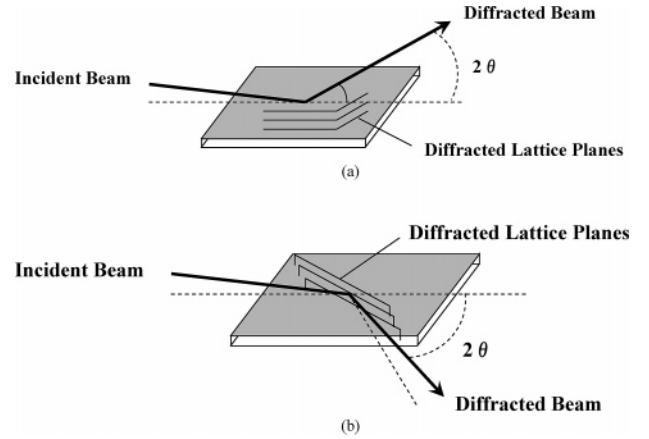

Figure 1. Schematic of out-of-plane (a) and in-plane (b) GIXD configurations.

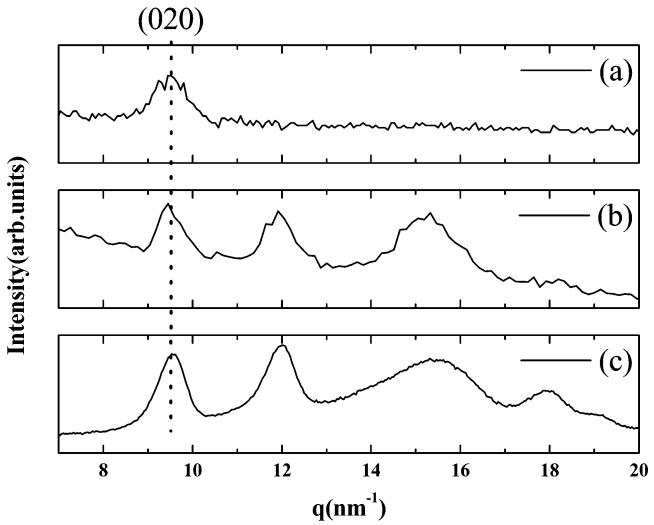

Figure 2. (a) Out-of-plane and (b) in-plane GIXD profiles of a 75 nm thick P(HB-*co*-HHx) film. (c) A WAXD profile of bulk P(HB-*co*-HHx) sample. Cu Kα_1 radiation (λ = 0.154 05 nm) is used for (a) and (c), whereas X-ray with wavelength of 0.080 nm is used for (b). Incident angles of X-ray beam are 0.61° (=3.8θ_c) in (a) and 0.32° (=3.8θ_c) in (b). The vertical dotted line indicate the peak position of (020) Bragg reflection.

fibers are greatly influenced by structure and morphology in their surface region.

In the present study we focus on the morphology and crystalline structure of P(HB-*co*-HHx) and PHB thin films ranging from 20 to 120 nm thick. Thermal behavior is investigated by two surface-sensitive X-ray scattering techniques: X-ray reflectivity (XR) and grazing incidence X-ray diffraction (GIXD). From XR and additional ex-situ AFM measurements, surface morphology of spin-coated PHB films is found to be substantially different from that of P(HB-*co*-HHx) for films with thickness greater than a critical vale. From GIXD, we find that the crystallographic *b*-axis of crystallites in an outermost surface region is highly aligned along the direction normal to the surface. Moreover, upon a heating and cooling, the *b*-axis in the surface region exhibits a noticeable thermal behavior. It indicates a novel molecular folding process which would be crucial for understanding physical properties of semicrystalline polymer surfaces.

Experimental Section

Bacterially produced PHB and P(HB-*co*-HHx) (HHx = 12 mol %, bulk melting temperature $T_m \sim 122$ °C) were obtained from the Procter & Gamble Co. They were purified by dissolving in hot chloroform, reprecipitated in methanol, and vacuum-dried at 60 °C. After dissolved in hot chloroform, PHB and P(HB-*co*-HHx) solutions were spun-cast onto silicon (100) wafers with a speed of 4000−4500 rpm. Spin-coated layers having 20 nm thickness and 120 nm thickness were prepared on the substrates from the solution with concentration of 6 mg/cm^3 and that of 12 mg/cm^3, respectively. Detailed information on film preparation is listed in Table 1. GIXD and XR measurements were carried out within 5 days after the coating.

As the index of refraction in X-ray regime is slightly smaller than unity, total external reflection occurs when the incident angle of X-ray impinging on a sample surface is smaller than a critical angle of total reflection θ_c. Since the penetration depth of X-ray drastically changes from several nanometers to several micrometers over the critical angle, surface-sensitive Bragg reflection profiles can be obtained under a precise control of the incident angle of X-ray beam. Detector scans were used to collect GIXD data with fixed grazing incident angle. More specifically, GIXD measurements in this study were performed with an out-of-plane configuration and an in-plane configuration to detect the crystalline structure of parallel and perpendicular to the substrate, respectively (Figure 1). On the other hand, longitudinal scans were exploited for measuring the XR which is capable of evaluating film thickness, electron density, and root-mean-squares of surface and interface roughness.[19] Measurements of GIXD and XR at room temperature were conducted by a high-resolution four-circle diffractometer and rotating-anode X-ray generator (SLX-2000&UltraX, Rigaku Co., Ltd., X-ray wavelength = 0.154 05 nm, θ_c = 0.162°). In order to obtain information about the crystalline structure in an outermost surface region during heating and cooling processes, synchrotron radiation (X-ray wavelength = 0.08 nm, θ_c = 0.084°) and a multiaxis diffractometer equipped at BL13XU of SPring-8 were employed.[20,21] Sample temperature, ranging from room temperature to the temperature close to the melting point of P(HB-*co*-HHx) was controlled by combination of a homemade heater and a PID temperature controller with the stability better than 0.3 °C. During the experiments, samples were kept under a helium gas atmosphere to prevent from the surface oxidation. Surface morphology was also observed by AFM at room temperature (Nanopics2100, SII Nano Technology Inc.).

Results and Discussion

I. Crystal Orientation. Figures 2a,b show GIXD profiles of a 75 nm thick P(HB-*co*-HHx) film, whereas Figure 2c is a WAXD profile obtained from a bulk sample under normal setting conditions ($\theta-2\theta$ setting). In the GIXD, the angle of incidence is set to be 3.8θ_c, where the incident X-ray fully penetrates the polymer film so as to show preferred orientation in the whole film. Magnitude of momentum transfer q is defined as $4\pi \sin \theta/\lambda$, using wavelength λ and half of the scattering angle θ. The out-of-plane GIXD profile (Figure 2a) is quite different from the in-plane GIXD profile (Figure 2b), although the latter (Figure 2b) is somewhat similar to the WAXD profile of the bulk sample (Figure 2c). In the out-of-plane geometry only the (020) Bragg reflection is observed at q = 9.5 nm^{-1}, indicating that the *b*-axis of crystallites in the thin layer is almost aligned in direction normal to the film surface. On the other hand, crystallites are much more isotropic in the lateral direction, since other Bragg reflections are also observed in the in-plane GIXD profile. Such a preferred orientation in thin films would reflect a difference in surface energy among crystallographic planes. Surface energy of the (010) plane is likely to be lower than that of (001) and (100) planes; the speed of crystal growth along the *b*-axis direction is thus expected to be the lowest. Such a result on preferred orientation of lamellae in the surface region is fully consistent with the studies of bulk structures, from which the anisotropic feature of molecular interaction was

Table 1. Concentration (mg/cm^3) and Rotation Speed (rpm) for Preparing the Thin Layers and Thickness (nm) Obtained

	PHB		P(HB-*co*-HHx) (HHx = 12 mol %)		
concentration (mg/cm^3)	6	12	6	12	12
rotation speed (rpm)	4500	4000	4500	4500	4000
thickness (nm)	30	unknown	35	75−82	111

clearly elucidated:[12−14] From the distance between adjacent molecules in crystalline lamellae, intermolecular interaction along the *b*-axis should be a weak van der Waals interaction. On the other hand, the (001) surface would be less favorable because the *c*-axis is the so-called fiber axis.[6,7] As for the *a*-axis direction, a unique hydrogen bonding of C−H···O═C type connecting the CH_3 group in one helix and the C═O group in another helix along the *a*-axis has been proposed.[12−14] If such a hydrogen bond network still dominates at the surface, forming the (100) surface would be energetically less favorable, and consequently the *a*-axis direction would be the fastest lamella-growth direction. The result of the present study may thus provide another supporting evidence for the hydrogen bonding proposed in refs 12−14. As for the PHB thin films, the same preferred (010) orientation was also confirmed by the present GIXD measurements, which completely agrees with the results reported in ref 16. From the width of Bragg reflections in Figures 2b,c we estimate the average dimensions of crystallite in the film and that in bulk to be around 12 and 19 nm, respectively.

II. Temperature Dependence. In order to explore thermal behavior of P(HB-*co*-HHx) molecules in the surface region, high-resolution measurements of the (020) Bragg reflection were performed under GIXD conditions. Figure 3 depicts a temperature-dependent variation in diffraction profiles around (020) Bragg reflection over a temperature range from 30 to 116 °C. The profile collected at 30 °C after a rapid cooling from 116 °C (cooling rate = 1 °C/min) is also shown at the top of Figure 3. Thickness and root-mean-square surface roughness of the film evaluated by XR at room temperature are 82.8 and 6.3 nm, respectively. Since the angle of incidence is chosen to be $0.95\theta_c$, the penetration depth of incident X-ray should be about 30 nm, which is smaller than the layer thickness. GIXD profiles in Figure 3 thus reflect the crystal structure only in the outermost-surface region. The high-resolution measurements reveal some marked aspects on the *b*-axis length of lamellar crystallites in the surface region. The most striking points seen in Figure 3 are the two resolved reflections at the position where (020) Bragg reflection is observed and their temperature evolutions. Since the WAXD pattern in Figure 2c agrees with the GIXD pattern in Figure 2b, indicating that the space group and crystal structure of lamellae distributed in thin films would be identical to those in the bulk polymer, and there is no valid Brag reflection except for (020) in this angular region, it is very likely that the two resolved reflections are (020) reflections diffracted by two orthorhombic crystalline lattices having slightly different *b*-axis lengths. Bragg reflections except for (020) reflection should appear in the region $q > 11$ nm^{-1}, since the *a*-axis length and *c*-axis length are almost half of the *b*-axis length. The (020) reflection at $q = 9.3$ nm^{-1} (we shall call it $(020)_L$) almost disappears at 46 °C. On the other hand, the $(020)_H$ reflection seen at $q = 9.9$ nm^{-1} becomes a well-defined peak above 46 °C, although it looked like a shoulder of $(020)_L$ at 30 °C. The $(020)_H$ reflection is still observed at 116 °C, which is slightly below the bulk melting point. After a rapid cooling, the $(020)_H$ reflection seems to remain, whereas the intensity of $(020)_L$ reflection drastically increases as indicated by the top profile in Figure 3.

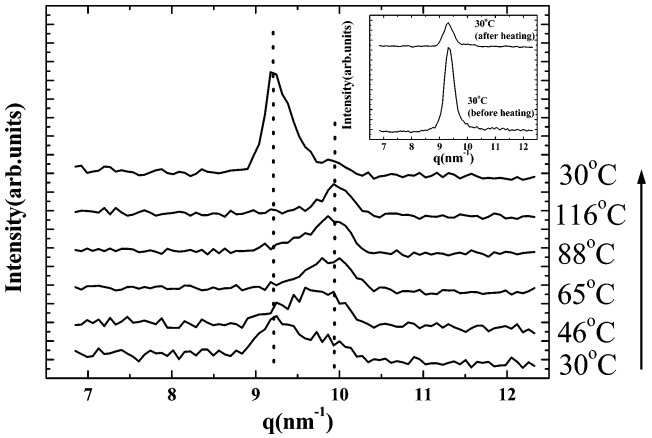

Figure 3. Temperature dependence of (020) Bragg reflection of P(HB-*co*-HHx) under out-of-plane GIXD condition measured at an incident angle of 0.08° (=$0.95\theta_c$). Each data is shifted vertically for clarity. The measurement was done with increasing the sample temperature. The profile of 30 °C shown at the top is the one quenched from 116 to 30 °C. The vertical dotted lines indicate the peak positions of two (020) reflections. The inset shows the GIXD at an incident angle = 0.09° (=$1.07\theta_c$), which indicates volume fraction of crystalline lamellae in bulk region; it shows a sharp contrast with the data obtained by the grazing angle of 0.08° (=$0.95\theta_c$), which reflects the crystallinity in the very shallow surface region.

We also confirmed the $(020)_L$ and $(020)_H$ reflections and studied their thermal behavior under the incident angle of $1.07\theta_c$ (=0.090°). Here, ratio of the initial $(020)_L$ intensity to the intensity of $(020)_L$ after the rapid cooling is quite different. The ratio is about 1:1.5 for the data with the incident angle of $0.95\theta_c$. On the other hand, it is about 1:0.3 in the case of the incident angle of $1.07\theta_c$, as is seen in the inset of Figure 3. From the well-resolved $(020)_H$ and $(020)_L$ reflections, it is unlikely that the two orthorhombic lattices with different *b*-axis lengths coexist in each crystallite. If such slightly larger lattices and slightly smaller lattices were randomly distributed in a single crystallite, (020) reflection would not split up into two resolved peaks, but the width of (020) reflection would simply increase. Therefore, we can conclude that there are at least two kinds of crystallites of some dimensions: one has a shorter *b*-axis (b_{Short}), and other has a longer *b*-axis (b_{Long}). From the peak position of $(020)_L$, b_{Long} was estimated as 1.35 nm, and b_{Short} was estimated as 1.27 nm from the position of $(020)_H$ peak. Since PHB is known to form lamellar crystals,[9,14] the present result indicates that there are loosely packed lamellae in which molecules are folded rather loosely and densely packed lamellae where the molecules are densely packed in them; loosely packed lamellae and densely packed lamellae are characterized by b_{Long} and b_{Short}, respectively. Since the *b*-axis length of bulk PHB often shows some irreproducibility after heating and subsequent cooling processes, inter- and intramolecular interactions along *b*-axis are considered to be extremely weak, and the *b*-axis length is expected to be easily affected by the situation around the crystallite.[14] Thus, a careful examination of b_{Long} and b_{Short} would give us important information on circumstances during the lamellae growth, e.g., molecular chain folding in the surface region. In order to see the volume fraction of loosely packed lamellae and densely packed lamellae quantitatively, we fitted

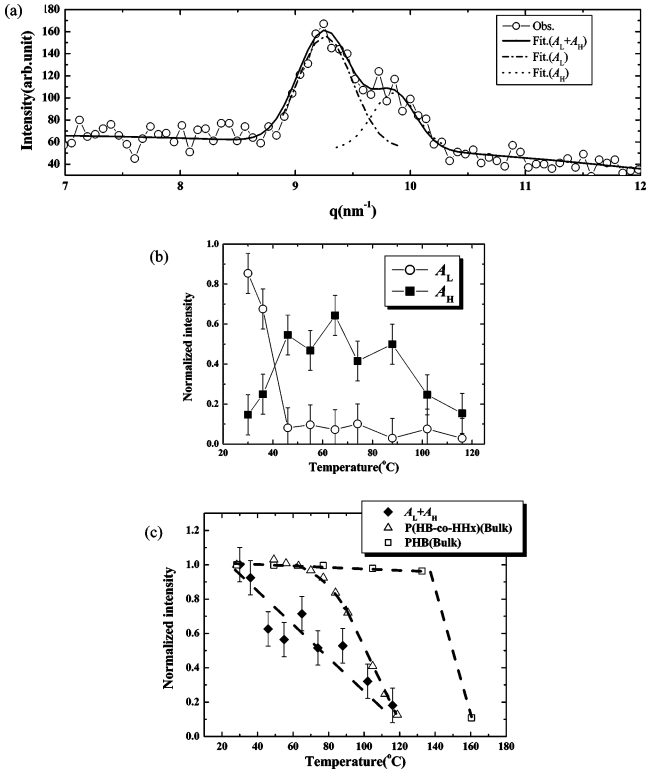

Figure 4. (a) An example of (020) Bragg reflection profile of P(HB-*co*-HHx), measured at room temperature with an incident angle of 0.08° (=0.95θ_c). (b) Fitted A_L (open circles) and A_H (closed squares) of P(HB-*co*-HHx) vs temperature. (c) Normalized intensities of (020) Bragg reflection of P(HB-*co*-HHx) thin film (= $A_L + A_H$), bulk P(HB-*co*-HHx) and bulk PHB. The solid curve drawn in (a) indicates the fit of eq 1 in the text. Dash-dotted and dotted curves are numerically calculated $A_L \exp(-\alpha_L(q-q_L)^2)$ and $A_H \exp(-\alpha_H(q-q_H)^2)$ by using the fitted parameters, respectively. In (b), A_L and A_H are normalized as A_L(30 °C) + A_H(30 °C) = 1. In (c), no intensity correction for illuminating volume has been made. Instead of the correction, intensity is set to be unity at room temperature so as to show the temperature dependence effectively. Error bars are not indicated for the intensities of bulk samples, since they are smaller than the size of symbols in this figure.

the intensity distribution around the two (020) reflections, $I(q)$, as a sum of two Gaussian functions:

$$I(q) = aq^2 + bq + c + A_L \exp(-\alpha_L(q - q_L)^2) + A_H \exp(-\alpha_H(q - q_H)^2) \quad (1)$$

where a, b, c, A_i, α_i, and q_i (i = L, H) are the fitting parameters. The quadratic function portion $aq^2 + bq + c$ in (1) sufficiently reproduced the background scattering. Figure 4a shows profiles of the two (020) reflections and the result of fittings. The temperature dependences of A_L and that of A_H, proportional to the intensity of $(020)_L$ and that of $(020)_H$, are shown in Figure 4b where they are normalized as $A_L + A_H = 1$ at room temperature. It quantitatively delineates temperature evolutions of $(020)_L$ and $(020)_H$. Although values of A_L and A_H drastically change between 30 and 50 °C, the decrease in A_L almost corresponds to the increase in A_H. This result strongly suggests that a transformation from loosely packed lamellae to densely packed lamellae occurs in this temperature range. Since loosely packed lamellae easily transform to densely packed lamellae by changing their packing ratio in lamellae, it is quite likely that loosely packed lamellae are in a metastable state, in which they might contain more structural disorder in molecular chain folding. Loosely packed lamellae would have a strong tendency

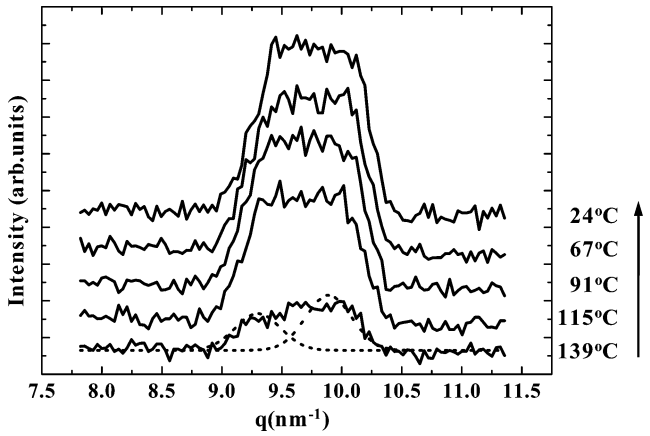

Figure 5. Temperature dependence of (020) Bragg reflection of P(HB-*co*-HHx). Measurement was done under out-of-plane GIXD setting with a cooling rate of 0.05 °C/min. For clarity, each diffraction profile is shifted vertically. Unlike the measurement under the rapid cooling (Figure 3), a low-resolution mode was adopted because of the conventional X-ray source with 18 kW where we use X-rays much weaker than those at synchrotron radiation facilities. Dotted curves are $(020)_L$ and $(020)_H$ reflections at 139 °C obtained by fitting. From the trapezoidal shape of the profile, $(020)_L$ and $(020)_H$ appear to grow equally under the slow cooling, which exhibits a sharp contrast with the results shown in Figure 3.

to transform to more stable state with high-density, i.e., densely packed lamellae, when they get sufficient thermal energy to get over a potential barrier between the metastable state and the stable state in their energy landscape. The transformation should occur stochastically at any temperature if it is above the glass transition temperature (ca. 0 °C). However, even at room temperature, it should take a longer period of time. It would be better to remind the fact that 2 or 3 days are insufficient for completing the crystallization in bulk PHB at room temperature. On the other hand, the densely packed lamellae are still stable even at around 60 °C, but they eventually decrease their volume over 80 °C. According to Figure 4c, the sum of $(020)_L$ and $(020)_H$ intensities (= $A_L + A_H$) steadily decreases above 30 °C. This means that the melting process of crystallites in the surface region continuously proceeds, although crystallites in the bulk region seem to sustain its structure up to 60 °C for P(HB-*co*-HHx) and up to 140 °C for PHB. Such a continuous fashion of lamellae melting would be due to the melting of small crystallites distributed in the surface region, although there is some possibility that it can be due to the surface melting phenomenon inherent in quasi-2D systems reported in many nonpolymeric crystals.[22]

Since loosely packed lamellae in the surface region are easily formed even under the quenching from high temperature, loosely packed lamellae are likely to be produced by an additional process which strongly promotes the crystalline long-range order in the surface region. Our speculation that major location of loosely packed lamellae is in the surface region is verified if we carefully look at the diffraction profiles in Figure 3 and the inset. With the very shallow incident angle (0.95θ_c), the $(020)_L$ is greatly enhanced by the quenching, whereas it did not show such an enhancement when we measured the same reflection with the larger incident angle (1.07θ_c: inset). Since the diffraction profile with the incident angle of 1.07θ_c fully represents the crystallinity in bulk region, the inset would manifest that loosely packed lamellae hardly form in the bulk region under the rapid cooling condition.

Figure 5 shows development of (020) reflections of P(HB-*co*-HHx) under a slow cooling condition measured by SLX-2000&UltraX where a low-resolution measurement mode was

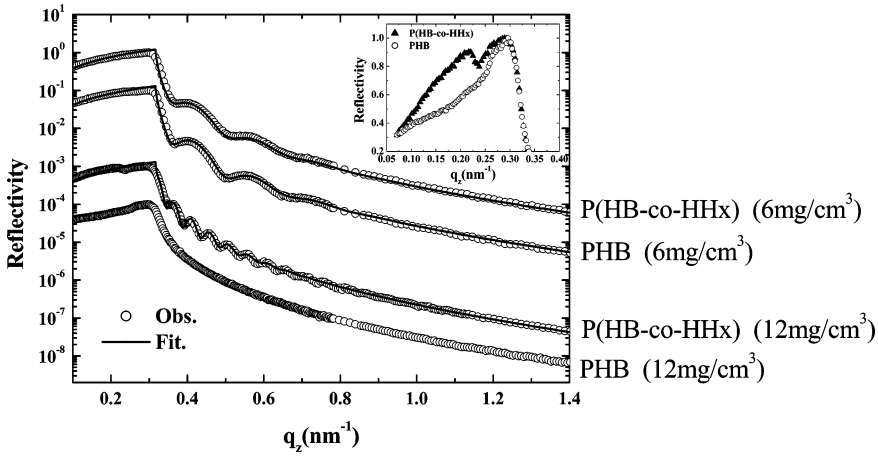

Figure 6. X-ray reflectivity of PHB and P(HB-*co*-HHx) thin films. Solid lines are the fitted curves. For clarity, each XR is shifted vertically and labeled by concentration. Inset shows a linear-scaled XR in the total reflection region of PHB and that of P(HB-*co*-HHx); both of them were prepared by solutions with concentration of 12 mg/cm^3.

adopted to gain the diffracted intensity. Because of the low-resolution mode, $(020)_L$ and $(020)_H$ are not resolved, but a broad trapezoidal peak is obtained. Two peaks could have been observed if a high-resolution mode had been adopted. At the highest temperature observed, a broad, slightly asymmetric (020) reflection which consists of $(020)_L$ and slightly strong $(020)_H$ reflections is observed (two dotted curves in Figure 5). It indicates that the probability of finding densely packed lamellae is larger than that of finding loosely packed lamellae at temperatures higher than room temperature, as is already confirmed in high-resolution measurements (Figure 3). In a subsequent slow cooling (cooling rate = 0.05 °C/min), we find that loosely packed lamella and densely packed lamella equally form since the reflection grows by keeping the trapezoidal shape (Figure 5). This result shows a sharp contrast with the result under the rapid cooling condition in which densely packed lamellae hardly formed throughout the quenching (Figure 3). Since crystallization of quenched bulk PHB is known to proceed for about 1 week at room temperature, the cooling rate of 1 °C/min adopted in the measurement shown in Figure 3 can be regarded as a rapid cooling (i.e., (116 °C − 30 °C)/(1 °C/min) < 2 h). In comparison with the cooling rate of 1 °C/min, the cooling process with the speed of 0.05 °C/min may rather be a quasi-equilibrium process because it took more than 36 h from 139 °C to room temperature. If the reason for forming only loosely packed lamellae after the rapid cooling is the lack of the annealing time for loosely packed lamellae to transform to densely packed ones, the result of slow cooling can naturally be understood. Namely, during the slow cooling, about half of loosely packed lamellae could acquire enough thermal energy to get over the potential barrier to the stable state where the densely packed lamellae occupy. It is thus strongly expected that no loosely packed lamellae would be obtained in thermal equilibrium. We consider that this is the first experimental results on a novel surface effect which is responsible for the metastable crystalline lamellae hardly observed in the structural studies on bulk polymers. Formation of loosely packed lamellae under the rapid cooling suggests that the mobility of molecules in the surface region would substantially be higher than that in the bulk region. The continuous fashion of lamellae melting at the surface may support the high mobility in the surface region, although we do not intend to exclude other possibilities for molecular ordering at the surface, e.g., an epitaxial effect due to the confined geometry. Further study like a direct measurement of mobility or diffusion coefficient in the surface region is certainly needed to determine the mechanism of loosely packed lamellae formation and transformation to densely packed lamellae on a microscopic level.

III. Surface Morphology of PHB and P(HB-*co*-HHx). The relationship between surface morphology of PHB and film thickness has already been investigated using XR, GIXD, and AFM in ref 16. In this study, we measured XR and AFM of P(HB-*co*-HHx) as well as PHB to see how the slight difference in molecular structure can affect the surface morphology of thin films. In Figure 6, a clear Kiessig fringe pattern is observed in XR of the two P(HB-*co*-HHx) films. Since the fringe pattern is caused by interference of X-rays reflected from the film surface and the substrate surface, we can obtain film thickness and parameters on the surface and interface roughness. From the standard fitting procedure,[23] thickness d and surface roughness σ are evaluated as d = 34.5 nm, σ = 3.8 nm for P(HB-*co*-HHx) film prepared from solution with concentration of 6 mg/cm^3, and d = 111.0 nm, σ = 4.7 nm for P(HB-*co*-HHx) from solution of 12 mg/cm^3. The PHB film prepared from solution of 6 mg/cm^3 concentration also exhibits the fringe pattern yielding d = 30.0 nm and σ = 3.4 nm. On the other hand, for the PHB film prepared from the solution with concentration of 12 mg/cm^3 which should be expected to have almost the same thickness as the corresponding P(HB-*co*-HHx) film, no fringe pattern is observed. Furthermore, XR of PHB (12 mg/cm^3) exhibits a steeper decrease in higher q_z region than the curve of the Fresnel reflectivity in which a perfectly flat surface was assumed (not plotted). Since large surface roughness can easily destroy the interference pattern and greatly reduce the intensity in XR, Figure 6 indicates that a flat and coherent surface is not formed for thicker PHB film (12 mg/cm^3). This observation is also confirmed from the inset of Figure 6, in which the enlarged linear-scaled XR data depicted around the total reflection regime (q_z < 0.3 nm^{-1}) is shown: On the XR of P(HB-*co*-HHx), a distinct peak is seen at q_z = 0.22 nm^{-1}, which corresponds to the calculated critical momentum transfer q_c (= $4\pi \sin \theta_c/\lambda$) for total reflection of P(HB-*co*-HHx). It indicates that the surface of P(HB-*co*-HHx) film is fairly flat and quite parallel to the Si substrate. It exhibits a sharp contrast with that of PHB. There is no peak around $q_z = q_c$ in the XR of PHB, but some reduction is recognized for q_z < 0.27 nm^{-1}. We consider that the loss of intensity under such very shallow incident angles comes from the rough and jugged surface morphology on the thick PHB film. This speculation is fully consistent with the discussion on the XRs in $q_z > q_c$.

Figure 7 displays AFM images of a P(HB-*co*-HHx) film with d = 111.0 nm and a corresponding PHB film. Surface

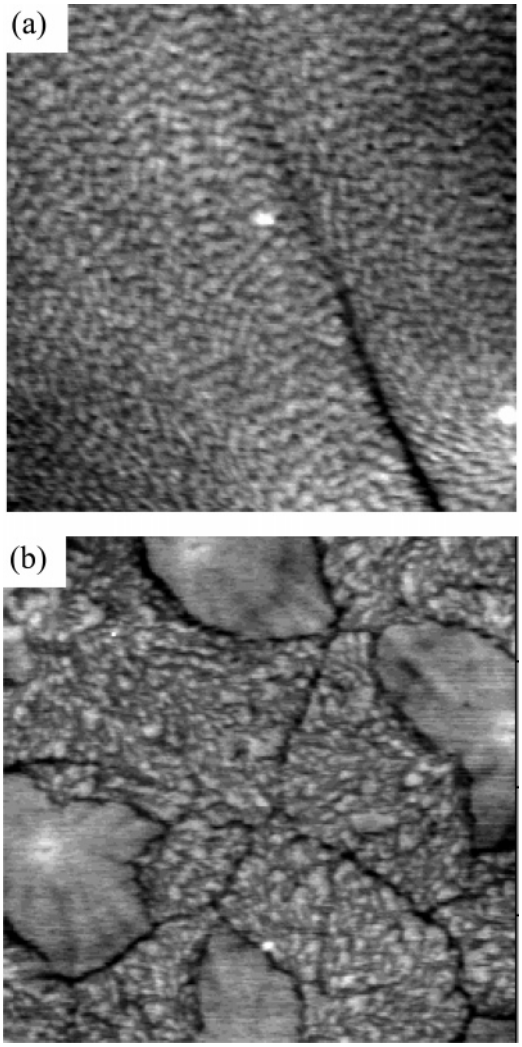

Figure 7. AFM images of (a) P(HB-*co*-HHx) and (b) PHB films made from solutions with a concentration of 12 mg/cm^3. Size of the image is 20 μm $\times$ 20 μm in area. Thickness of the films is about 111 nm.

morphology of the PHB film looks very dissimilar to that of the corresponding P(HB-*co*-HHx) film. On the PHB surface, two kinds of polygonal domains coexist. The one has a fine texture that is also seen in the image of P(HB-*co*-HHx); another has no fine structure in it but looks like a hillock pointed upward. It is quite likely that one of them can be attributed to spherulites truncated at the surface, since huge spherulites are often observed in bulk PHB samples prepared from melt. However, it might be better not to leap to the conclusion; as far as the authors know from the experiments at room temperature, no spherulite has formed in PHB dried from the chloroform solutions dropped on glass substrates. From XR and AFM, surface morphology of PHB and P(HB-*co*-HHx) was found to be very similar to each other when the film thickness is less than 50 nm (not shown). Therefore, the different morphology inherent to each material would emerge only for the films thick enough where effects from the polymer/Si interface would fully be ignored. It may seem rather inexplicable if we recall the slight difference in molecular structure between PHB and P(HB-*co*-HHx). We consider that the high crystallinity of PHB would be one of the origins on the difference in surface morphology between homopolymers and random copolymers. Crystalline lamellae on PHB surface might hinder the uniform surface morphology, although we do not say whether the spherulites form in the PHB ultrathin films or not.

Controlling the crystallinity in semicrystalline polymers has been one of the key issues in practical applications, since the crystallinity greatly affects many mechanical properties in polymeric substances. PHAs may become too brittle, presumably due to the crystallites embedded in amorphous matrix. We think we may shed a light on to this problem from a different standpoint. Since loosely packed lamellae are found to easily form even during the rapid cooling, formation of a surface with high coverage of crystalline lamellae seems to be inevitable. Such loosely packed lamellae would eventually transform to more stable, densely packed lamellae which would be in the lower energy state at an ambient temperature. Once the crystallites find a way to the stable state in their energy landscape, the energy difference between amorphous and densely packed lamellae may act as a driving force for expanding the volume of stable crystalline lamellae into the adjacent amorphous matrix. On a free surface like this, part of crystallization may extend inward like other glass forming nonpolymeric materials at above their glass transition temperatures.[18] Controlling the crystallinity in the surface region would thus become a technologically critical and challenging issue which determines the physical properties of PHAs, especially for thin films and fibers. Relationship between crystallinity and morphology at the surface for various HHx concentrations and their temperature dependence are open questions, which should certainly become crucial for controlling the physical properties in the surface region as well as those in the bulk region.

Summary

Surface structure and thermal properties of PHB and P(HB-*co*-HHx) thin films are investigated by GIXD and XR with conventional X-ray and synchrotron radiation. Preferred orientation of crystallites in thin films is confirmed for both polymers. An origin of surface-induced preferred orientation is explained by C−H···O═C hydrogen bonding. Moreover, lamellae in the surface region are found to be classified by stable and metastable types. Novel crystallization process peculiar to the surface region, in which transformation from metastable lamellae to stable ones is a key phenomenon, is proposed. Different surface morphology between PHB and P(HB-*co*-HHx) films is studied by XR and AFM, most likely reflecting the difference in crystallinity in the surface region.

Acknowledgment. We express our great thanks to Drs. A. Kitahara and O. Sakata for ceaseless support and helpful advice during the measurements. Part of the research was financially supported by The Promotion and Mutual Aid Corporation for Private Schools of Japan (The Science Research Promotion Fund in 2006 and 2007). The synchrotron radiation experiments were performed at BL13XU in SPring-8 with the approval of the Japan Synchrotron Radiation Research Institute (JASRI) (Proposal Nos. 2005A0094-ND1d-np, 2005B0451, and 2006A1426).

References and Notes

(1) Doi, Y. *Microbial Polyesters*; VCH Publishers: New York, 1990.
(2) Anderson, A. J.; Dawes, E. A. *Microbiol. Rev.* **1990**, *54*, 450.
(3) Chiellini, E.; Solaro, R. *Recent Advances in Biodegradable Polymers and Plastics*; Wiley-VCH: Weinheim, 2003.
(4) Alper, R.; Lundgren, D. G.; Marchesssault, R. H.; Cote, W. A. *Biopolymers* **1963**, *1*, 545.
(5) Lundgren, D. G.; Alper, R.; Schnaitman, C.; Marchessault, R. H. *J. Bacteriol.* **1965**, *89*, 245.
(6) Yokouchi, M.; Chatani, Y.; Tadokoro, H.; Teranishi, K.; Tani, H. *Polymer* **1973**, *14*, 267.
(7) Cornibert, J.; Marchessault, R. H. *J. Mol. Biol.* **1972**, *71*, 735.
(8) Doi, Y.; Kitamura, S.; Abe, H. *Macromolecules* **1995**, *28*, 4822.

(9) Abe, H.; Doi, Y.; Aoki, H.; Akehata, T. *Macromolecules* **1998**, *31*, 1791.
(10) Marcott, C.; Dowrey, A. E.; Poppel, J. V.; Noda, I. *Vib. Spectrosc.* **2004**, *36*, 221.
(11) Web site: www.nodax.com.
(12) Sato, H.; Nakamura, M.; Padermshoke, A.; Yamaguchi, H.; Terauchi, H.; Ekgasit, S.; Noda, I.; Ozaki, Y. *Macromolecules* **2004**, *37*, 3763.
(13) Sato, H.; Murakami, R.; Padermshoke, A.; Hirose, F.; Senda, K.; Noda, I.; Ozaki, Y. *Macromolecules* **2004**, *37*, 7203.
(14) Sato, H.; Mori, K.; Murakami, R.; Ando, Y.; Takahashi, I.; Zhang, J.; Terauchi, H.; Hirose, F.; Senda, K.; Tashiro, K.; Noda, I.; Ozaki, Y. *Macromolecules* **2006**, *39*, 1525.
(15) Padermshoke, A.; Sato, H.; Katsumoto, Y.; Ekgasit, S.; Noda, I.; Ozaki, Y. *Vib. Spectrosc.* **2004**, *36*, 241.
(16) Capitán, M. J.; Rueda, D. R.; Ezquerra, T. A. *Macromolecules* **2004**, *37*, 5653.
(17) Frenken, J. W. M.; van der Veen, J. F. *Phys. Rev. Lett.* **1985**, *54*, 134. Bilgram, H. *Phys. Rep.* **1987**, *153*, 1. Prince, K. C.; Breuer, U.; Bonzel, H. P. *Phys. Rev. Lett.* **1988**, *60*, 1146.
(18) Kikkawa, H.; Kitahara, A.; Takahashi, I. In *Slow Dynamics in Complex Systems*; Tokuyama, M., Oppenheim, I., Eds.; American Institute of Physics: Melville, NY, 2004; Vol. 708, p 619.
(19) Tolan, M. *X-Ray Scattering from Soft-Matter Thin Films*; Springer: Berlin, 1999.
(20) Sakata, O.; Furukawa, Y.; Goto, S.; Mochizuki, T.; Uruga, T.; Takeshita, K.; Ohashi, H.; Ohata, T.; Matsushita, T.; Takahashi, S.; Tajiri, H.; Ishikawa, T.; Nakamura, M.; Ito, M.; Sumitani, K.; Takahashi, T.; Shimura, T. A. Saito; Takahashi, M. *Surf. Rev. Lett.* **2003**, *10*, 543.
(21) Yakabe, H.; Tanaka, K.; Nagamura, T.; Sasaki, S.; Sakata, O.; Takahara, A.; Kajiyama, T. *Polym. Bull. (Berlin)* **2005**, *53*, 213.
(22) Stoltze, P.; Norskov, J. K.; Landman, U. *Phys. Rev. Lett.* **1988**, *61*, 440; *Surf. Sci.* **1989**, *220*, L693.
(23) Parratt, L. G. *Phys. Rev.* **1954**, *95*, 359.

MA7020858